

# Photophysical Properties of Protonated Aromatic Hydrocarbons

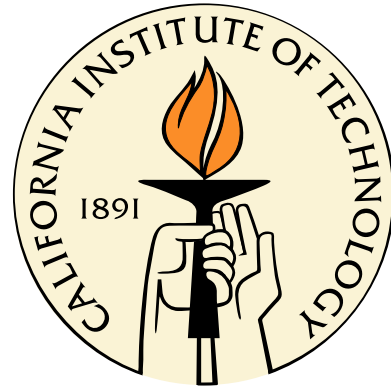
Thesis by

Vadym A. Kapinus

In Partial Fulfillment of the Requirements

for the Degree of

Doctor of Philosophy



California Institute of Technology

Pasadena, California

2005

(Defended December 14, 2004)

© 2005

Vadym A. Kapinus

All Rights Reserved

# Acknowledgements

I have greatly enjoyed the years I have spent at Caltech and it will be hard to express my thanks to the many people to whom I am indebted to for such unforgettable experiences.

First, I was fortunate to have Professor Geoffrey Blake as my research advisor. I appreciate the energy, enthusiasm and support that Geoff provided during my graduate career. The door of his office was always open for students, he always welcomed new ideas, and would have a few suggestions when the experiment did not work. Most of all, I value the freedom that Geoff gave me in conducting research. I would also like to thank Professors Jack Beauchamp and Mitchio Okumura for some of the discussions I had with them.

When I joined the Blake group, I was working closely on the experiments with Sheng Wu and Zulfikar Morbi. I learned many things about non-linear optical devices from Sheng, and later I had a long collaboration with him on a number of tunable solid state light sources. Zulf and I worked on the carbon chain project, and from him I learned many useful things about lab management and experimental techniques. He was also the one who started me on programming the remote control of digital oscilloscopes, which later became the main part of my data collection software. Susanna Widicus-Weaver helped me in my attempt to record the microwave spectrum of protonated benzene. Michael Morton was the beta tester for the BGSpecT software.

The Blake group was an interesting place to work and I would like to thank some of its

former and current members for providing a friendly working environment, and for lending a hand or a good word when I needed them: Susanna, Mike, Zulf, Sheng, Hui Zhang, Zifu Wang, François Jeanneret, Rogier Braakman and Daniel Holland.

Administrative assistants, Janis Haskell and Leticia Calderon from GPS division were very helpful with placing orders and solving some organizational questions. I would also like to acknowledge the help of the people from the Chemistry machine shop for their quality work on the parts for my experiment: Mike Roy, Guy Duremburg, Ray Garcia and Steven Olson. Tom Dunn from the Chemistry electronics shop was helpful with circuit designs and was generous with borrowing his high voltage probe. Tony Solyom from the Biology Division fixed a few chillers and vacuum pumps for me. I also enjoyed our long conversations on various topics. My thanks go to the Thaddeus group from Harvard for sharing their designs of the discharge source and the electronic circuitry for it.

With Andrei Deev, a longtime friend and roommate since my undergraduate years, I had many discussions about science and life in general. Ironically, we both ended up at Caltech, in the same department, and conducting research in related areas – even having our thesis defense scheduled on the same day!

Many other people at Caltech contributed to the quality of my non-academic life, and became my friends. Julia Lyubovitsky taught me quite a few subtle things about american culture, first when doing homework together and later, during our long lunch chats. Leo Eisner used my weakness for good food to introduce me to the sport of orienteering. Together, we had many unforgettable moments, especially at Mt. Piños, Redwoods, Lake Tahoe and the Sierras.

Ulyana Dyudina, Andrei Khodakovsky, Andrey Bereznyak and Dmitry Novikov were my buddies on hiking trips – from going up to the local mountains, to going down to the Grand

Canyon. They, and some other members of russian-speaking community (Andy Greenberg and Galina Lokshina, George Shapovalov and Kira Kostenko, Alexander Putilin, Vadim Borokhov, Alexei Dvoretskii, Ivan Mokhnal and Dmitry Kossakovski) did not allow me to lose the cultural connection with my homeland.

I would like to thank my soccer teammates from the Red Square and Kicking Buck teams, especially Jim Kempf, Lou Madsen and Gabriel Brandt.

I became a fan and a participant of another sport at Caltech: dancesport. Derrick Bass, the legendary guru of the Caltech Ballroom Dance Club, taught me my first steps. His thorough teaching style (what else can you expect from a theoretical physicist?) sparked my competitive spirit and interest in good technique. Our activities were not only limited to the dance floor with many other members of the ‘old’ team, including my first partner Meina Xu, Andreea Boca, Kok Win Goh, Joseph Chen, Christina Lam, Andrej Zlatos, Tammy Lam, Helen Claudio, Ania Kashina, Ulyana, Galka, Sasha. I also enjoyed working closely with the members of the CBDC organizing committee, especially Michael Fleming, Megan Ferguson and Keith Brown.

My dancing hobby profoundly changed my life by leading me to cross paths with my wife, Vanessa, who from just being a friend and dance partner became my best friend and partner in life. Her friendly words and warm smile gave me a lot of energy during the past two years. I express my great appreciation for her love, encouragement, patience and faith in me.

Finally, I would like to thank my family, especially my parents, Alexander and Nelya. They always provided me with freedom of choice and supported my interest in science, even when that interest led me to distant shores.

# Abstract

Diffuse interstellar bands (DIBs) were first observed in the visible region of the electromagnetic spectrum in the 1920s, with over a hundred features now discovered out to near-IR wavelengths. Since their initial discovery, many attempts have been made to identify the species that are responsible for the DIBs. Polycyclic aromatic hydrocarbons (PAHs) and their derivatives are among the likely candidates for DIB carriers, as demonstrated by the intense unidentified IR emission bands from  $3.3 - 11.3 \mu\text{m}$  that strongly point to their presence of aromatic species in the interstellar medium (ISM). The  $S_1 \leftarrow S_0$  electronic transitions for small PAHs lie in the near-UV, however, so only large neutral PAHs with 30+ carbon atoms can absorb at the visible wavelengths characteristic of the DIBs. In diffuse clouds and dense cloud envelopes that are exposed to the harsh interstellar radiation field, molecules are expected to be ionized. Positively charged PAHs are predicted to acquire a hydrogen atom to form thermodynamically stable protonated PAHs in diffuse clouds. These are closed-shell molecular ions with electronic transitions that are red-shifted compared to neutral PAHs, so even small protonated PAHs can, in principle, produce absorption bands in the visible.

Little is known about the photophysical properties of these compounds, however, so this thesis presents an experimental and theoretical analysis of two-, three-, and four-ring protonated PAHs. Theoretically, density functional theory calculations using the B3LYP

functional were used to study protonated PAHs in their ground electronic state. In particular, the energetics of the various potential protonated PAH isomers were calculated along with the proton tunneling or hopping barriers between them. The relative energies of the lowest lying photodissociation pathways were also calculated. It was found that the different isomers of protonated PAHs likely exist in thermodynamic equilibrium under interstellar conditions, thanks to the moderate ( $\sim 15 - 20$  kcal/mol) barriers to proton migration. Photochemically, the loss of an H atom or  $\text{H}_2$  molecule from a protonation site were identified as the most favorable dissociation channels for protonated PAHs. The H and  $\text{H}_2$  loss channels were found to be within a few kcal/mol of each other in energy, and about 45 – 60 kcal/mol above the ground state, depending on the parent molecule and isomer.

Following the ground state geometry optimizations and energy calculations, the Configuration Interaction Singles (CIS) method was used to estimate the positions of the electronic transitions for protonated PAHs. Depending on the PAH and isomer, red shifts up to 150 nm were predicted even for small systems, i.e., protonated naphthalene, anthracene, phenanthrene and pyrene. This places the  $S_1 \leftarrow S_0$  transitions of essentially all protonated PAHs well into the DIB wavelength region.

In order to investigate these predictions experimentally, a robust hydrogen discharge source was designed to produce protonated PAHs. Laser photodissociation of protonated PAHs was first studied with an excimer laser/reflectron time-of-flight mass spectrometer under ultrahigh vacuum conditions that mimic those in the ISM. Small protonated PAHs were found to be very photostable. Indeed, it was determined that nanosecond pulse length photodissociation is multiphoton even at short wavelengths (193 nm). For protonated anthracene, the dissociation limit was estimated to be 13 – 15 eV, which is much higher than the predicted thermodynamic threshold of 2.5 – 3.0 eV. This was attributed to the onset of

rapid intramolecular vibrational relaxation (IVR) upon electronic excitation.

Thanks to the excellent photostability of protonated PAHs, a cluster photodissociation approach was used to locate the electronic transitions of protonated anthracene between 420 and 540 nm. Clusters with water molecules were produced in a two-valve mixing discharge source. Visible photodissociation spectrum of these clusters was recorded using a novel optical parametric oscillator (OPO) with low beam divergence. The OPO utilizes a hybrid matching scheme involving BBO type I and II crystals in a rotated prism cavity. The observed protonated anthracene absorption bands are very wide (20 nm FWHM) – too wide to account for the DIBs. Again, this spectral broadening most likely results from rapid IVR induced by the high density of states in protonated PAHs. Such strong, wide bands may be important contributors to the overall visual extinction in the diffuse ISM and should efficiently produce infrared emission such as that seen in the Unidentified Infrared emission features, or UIRs.

# Contents

<b>Acknowledgements</b>	<b>iii</b>
<b>Abstract</b>	<b>vi</b>
<b>1 Protonated Polycyclic Aromatic Hydrocarbons and the Interstellar Medium</b>	<b>1</b>
1.1 Interstellar Molecules . . . . .	1
1.2 PAHs and the Unidentified IR Emission Bands . . . . .	3
1.3 The Diffuse Interstellar Bands . . . . .	4
1.3.1 Carbon Chains and the DIBs . . . . .	6
1.3.2 PAHs and the DIBs . . . . .	6
1.4 Protonated PAHs . . . . .	9
1.4.1 Protonated PAHs in ISM . . . . .	9
1.4.2 Protonated PAHs and the DIBs . . . . .	10
1.4.3 Other Applications of Protonated Aromatics . . . . .	11
1.4.4 Previous Studies of Protonated Aromatics . . . . .	11
1.5 Research Goals . . . . .	13
<b>2 Ground State Calculations for Protonated PAHs</b>	<b>15</b>
2.1 Introduction . . . . .	15
2.2 Methodology . . . . .	16

2.2.1	Naming Conventions . . . . .	16
2.2.2	Software . . . . .	17
2.2.3	Choice of the Computer System . . . . .	18
2.2.4	Theory Level and Basis Set . . . . .	19
2.3	Geometries . . . . .	21
2.3.1	Protonated Benzene, Naphthalene, Anthracene and Pyrene . . . . .	21
2.3.2	Typical Geometry Changes Upon Protonation . . . . .	27
2.3.3	Geometries of Dehydrogenated PAH Cations . . . . .	28
2.3.4	Geometries of Hydrogenated and Dehydrogenated PAHs . . . . .	28
2.4	Calculated Values . . . . .	29
2.4.1	Vibrational Frequencies . . . . .	29
2.4.2	Proton Affinities . . . . .	30
2.4.3	Ionization Energies . . . . .	31
2.5	Energy Landscapes . . . . .	32
2.5.1	Protonated Benzene . . . . .	33
2.5.2	Protonated Naphthalene . . . . .	34
2.5.3	Protonated Anthracene . . . . .	36
2.5.4	Protonated Phenanthrene . . . . .	38
2.5.5	Protonated Pyrene . . . . .	40
2.5.6	Hydrogenated PAHs . . . . .	41
2.6	Discussion . . . . .	44
2.6.1	Changes in the Vibrational Spectrum . . . . .	45
2.6.2	Proton Mobility . . . . .	46
2.6.3	Dissociation Channels . . . . .	47

2.6.4	Interstellar H <sub>2</sub> Formation	48
2.7	Summary	50
<b>3</b>	<b>Excited States Calculations for Protonated PAHs</b>	<b>52</b>
3.1	Introduction	52
3.2	Methodology	53
3.2.1	Theory Level and Basis Set	53
3.2.2	Convergence Tests	54
3.2.3	Scaling Factors	56
3.3	Valence Molecular Orbitals	57
3.3.1	Protonated Benzene	57
3.3.2	Other Protonated Aromatics	58
3.3.3	Electronic States Assignment	59
3.4	Excited States Energies	61
3.4.1	Comparison with DIB spectrum	64
3.5	Summary	65
<b>4</b>	<b>Experimental Setup</b>	<b>67</b>
4.1	Introduction	67
4.2	Pulsed Discharge Source	69
4.2.1	Design	69
4.2.2	Voltage and Current Profiles	72
4.2.3	Protonation Mechanism and Efficiency	73
4.3	Cluster Source	77
4.3.1	Design	77

4.3.2	Operation	78
4.4	Mass Spectrometer	79
4.4.1	Ion Shielding	80
4.4.2	Ion Extraction	81
4.4.3	Reflectron Mode	82
4.4.4	Detectors	83
4.4.5	Vacuum System	83
4.5	Laser Systems	84
4.5.1	Excimer Laser	84
4.5.2	Nd:YAG Lasers	85
4.5.3	BBO Type II OPO	85
4.6	Hybrid BBO OPO with a Rotated Prism Cavity	87
4.6.1	New Cavity Design	88
4.6.2	Phase Matching	88
4.6.3	The Choice of Crystals	90
4.6.4	Hybrid Cavity Performance	92
4.7	Other Hardware	94
4.8	Data Acquisition	95
4.8.1	Blake Group Spectroscopy Tools Software	95
4.8.2	Choice of Delay Times	96
4.8.3	Data Analysis	99
<b>5</b>	<b>Laser Dissociation of Protonated PAHs</b>	<b>100</b>
5.1	Experiments	100

5.1.1	The Type II BBO OPO as a Laser Photodissociation Source . . . . .	101
5.1.2	Two-color Dissociation – OPO and Excimer Laser . . . . .	102
5.1.3	Dissociation Yield with Excimer Laser . . . . .	103
5.2	Observed Results . . . . .	106
5.2.1	Photodissociation Products . . . . .	106
5.2.2	Yield Dependence on the Pulse Energy . . . . .	108
5.3	Discussion . . . . .	111
5.3.1	Multiphoton Nature of the Photodissociation . . . . .	111
5.3.2	Photostability and Implications for ISM . . . . .	113
5.4	Summary . . . . .	114
<b>6</b>	<b>Cluster Predissociation Spectroscopy of Protonated Anthracene</b>	<b>116</b>
6.1	Introduction . . . . .	116
6.2	Experiment . . . . .	117
6.3	Results and Discussion . . . . .	119
6.3.1	Cluster Geometry . . . . .	119
6.3.2	Measured Spectrum . . . . .	121
6.3.3	Band Positions and Widths . . . . .	123
6.3.4	Comparison with Spectra of Other Clusters . . . . .	124
6.3.5	Effect of Proton Mobility on the Spectral Width . . . . .	125
6.3.6	Other Factors . . . . .	126
6.3.7	Comparison with the DIBs . . . . .	127
6.4	Summary . . . . .	128
<b>7</b>	<b>Summary</b>	<b>130</b>

7.1	Structures and Reaction Pathways	130
7.2	Molecular Orbitals and Electronic Transitions	131
7.3	Photostability of Protonated PAHs	133
7.4	Visible Spectrum of Protonated Anthracene	134
7.5	Conclusions	135
7.6	Future Research Directions	135
<b>A</b>	<b>GAUSSIAN 98 Results</b>	<b>138</b>
A.1	Geometries	138
A.1.1	Z-Matrices	139
A.2	Vibrational Frequencies	156
A.3	Vibrational Spectra	169
A.4	Energy Landscapes for Protonated PAHs	179
A.5	Energy Landscapes for Hydrogenated PAHs	181
A.6	Ionization Energies	183
A.7	Excited States	184
<b>B</b>	<b>Experimental Setup Descriptions</b>	<b>191</b>
B.1	Discharge	191
B.1.1	Pulsed Discharge Source	191
B.1.2	Pulsed Discharge Cluster Source	198
B.2	Circuits	201
B.2.1	TTL Pulse Width Selector	201
B.2.2	Pulsed Valve Driver	202
B.2.3	TOF MS High Voltage Pulser	204

B.2.4 Frequency Divider . . . . .	206
<b>C Blake Group Spectroscopy Tools Software</b>	<b>208</b>
C.1 Main Panel . . . . .	208
C.1.1 Instruments . . . . .	209
C.1.2 Tools . . . . .	210
C.1.3 Menus . . . . .	210
C.1.4 System Tray Icon . . . . .	211
C.1.5 Other . . . . .	212
C.2 Lambda Tune Panel . . . . .	212
C.2.1 Remote Parameters Setup . . . . .	213
C.2.2 Lambda Tune Parameters . . . . .	214
C.2.2.1 Calibration File . . . . .	214
C.2.2.2 Wavelength Conversions . . . . .	218
C.2.2.3 Other Lambda Tune Parameters . . . . .	220
C.2.3 Changing Lambda Tune Wavelength . . . . .	221
C.3 Wavemeter Panel . . . . .	221
C.3.1 Remote Parameters Setup . . . . .	222
C.3.2 Wavemeter Parameters . . . . .	223
C.3.3 Reading Wavelength . . . . .	223
C.4 Motion Control Panel . . . . .	223
C.4.1 Remote Parameters Setup . . . . .	224
C.4.2 Motion Axes Parameters . . . . .	225
C.4.3 Moving Axes . . . . .	226

C.4.4	Positions File	227
C.5	Oscilloscope Panel	227
C.5.1	Remote Parameters Setup	227
C.5.2	Waveform Acquisition and Manipulation	230
C.5.2.1	Reading Waveforms	230
C.5.2.2	Viewing Waveforms	231
C.5.2.3	Saving Waveforms	232
C.5.3	Oscilloscope Parameters Setup	233
C.5.3.1	Panel Parameters	234
C.5.3.2	Common Scope Parameters	234
C.5.3.3	Channel Parameters	236
C.5.3.4	Channel Task Parameters	238
C.5.3.5	Save and Load Configuration	240
C.6	Delay Generator Panel	241
C.6.1	Remote Parameters Setup	241
C.6.2	Delay Generator Parameters	242
C.6.2.1	Trigger Parameters	243
C.6.2.2	Output Line Parameters	243
C.6.2.3	Delay Line Parameters	244
C.6.2.4	Save and Load Settings	245
C.6.3	Visualize Output Delay Pulses	245
C.7	Photon Counter Panel	246
C.7.1	Remote Parameters Setup	247
C.7.2	Photon Counter Parameters	248

C.7.2.1	Panel Parameters	248
C.7.2.2	Common Photon Counter Parameters	249
C.7.2.3	Counter Channel Parameters	249
C.7.2.4	Save and Load Settings	250
C.7.3	Reading Counts	251
C.8	Spectrum Scan Panel	251
C.8.1	Sources and Detectors	252
C.8.2	Sources Setup	252
C.8.3	Detectors Setup	256
C.8.4	Spectrum View	258
C.8.5	Other Features	260
C.8.6	Performing the Scan	262
C.9	Device Talk Panel	263
C.9.1	COM Port Settings	264
C.9.2	Talking to Devices	264
C.10	Devices	266
C.11	Device Setup	266
C.11.1	Create Device	267
C.11.2	Device Type	267
C.11.3	Device Communication Type	268
C.11.4	Device Communication Address	268
C.11.5	Turning Device On/Off	270
C.11.6	Panel Configuration Backup	270
C.11.7	Help	271

C.12 Readme . . . . .	271
C.13 License Agreement . . . . .	274
<b>Bibliography</b>	<b>277</b>

# List of Figures

1.1	A synthetic spectrum of the diffuse interstellar bands, based on the DIB compilation in [1]. The image is from [2].	5
2.1	Structures for protonated benzene PES stationary points. Adapted from [3].	15
2.2	Carbon atom numbering conventions for neutral PAHs.	17
2.3	Structures of protonated benzene $C_6H_7^+$ and its isomerization transition state 1–2 $C_6H_7^+$ .	22
2.4	Structures of the protonated naphthalene $C_{10}H_9^+$ isomers 1,2 and 9, along with three of the isomerization transition states that connect them.	23
2.5	Structures of the protonated anthracene $C_{14}H_{11}^+$ isomers 1, 2, 9 and 11, along with two of the lowest barrier isomerization transition states.	24
2.6	Structures of the protonated phenanthrene $C_{14}H_{11}^+$ isomers 1, 2, 3, 4 and 9.	25
2.7	Structures of the protonated pyrene $C_{16}H_{11}^+$ isomers 1, 2 and 4.	26
2.8	Benzene geometry changes (dashed line). 1 – during protonation, 2 – during cation dehydrogenation.	27
2.9	The energy landscape for protonated benzene.	33
2.10	The energy landscape of protonated naphthalene.	35
2.11	Protonated anthracene energy landscape.	37
2.12	A simplified version of the protonated phenanthrene energy landscape.	39

2.13	The energy landscape of protonated pyrene (not complete). . . . .	40
2.14	Hydrogenated benzene energy landscape. . . . .	41
2.15	Hydrogenated naphthalene energy landscape. . . . .	42
2.16	Hydrogenated anthracene energy landscape. . . . .	43
3.1	The $\pi$ molecular orbitals of benzene. . . . .	58
3.2	The $\pi$ molecular orbitals of protonated benzene. . . . .	59
3.3	Orthogonal axis selection for molecules with different symmetry. . . . .	60
3.4	Diffuse interstellar bands and calculated $S_1 \leftarrow S_0$ wavelengths for protonated PAHs. . . . .	64
4.1	The pulsed discharge source design. . . . .	70
4.2	Pulsed nozzle discharge voltage and current profiles. . . . .	72
4.3	Mass spectra of anthracene and protonated anthracene in He <i>vs.</i> H <sub>2</sub> discharges. . . . .	74
4.4	H <sub>3</sub> <sup>+</sup> formation and the protonation of different aromatic molecules (benzene, anthracene and pyrene) in hydrogen discharges. . . . .	75
4.5	Pulsed discharge cluster source with two pulsed valves. . . . .	77
4.6	The time-of-flight mass spectrometer setup for photodissociation experiments (top view). . . . .	80
4.7	A top view of the BBO type II OPO. . . . .	86
4.8	A top view of the BBO type I and II hybrid OPO with rotated prism cavity. . . . .	88
4.9	A rotated right angle prism. . . . .	89
4.10	The additional phase delay caused by an Al-coated BK-7 right angle prism. Calculated by Foreal Spectrum Co. . . . .	90
4.11	Light polarizations in a birefringent nonlinear crystal. . . . .	91

4.12	Beam shape for the mixed BBO type I and II prism cavity OPO. . . . .	93
4.13	Hybrid cavity OPO wavemeter reading at $\lambda_{\text{idler}} = 719$ nm. . . . .	93
5.1	An ion channel mass spectrum of protonated anthracene photodissociation with $\lambda = 193$ nm excimer laser pulses. . . . .	104
5.2	An ion channel mass spectrum of protonated pyrene photodissociation with $\lambda = 193$ nm excimer laser pulses. . . . .	104
5.3	Mass spectrum of the neutral products from protonated anthracene photodissociation. . . . .	105
5.4	Comparison of the linear mode mass spectra for protonated anthracene and its neutral photodissociation products. . . . .	105
5.5	Protonated anthracene photodissociation with $\lambda = 193$ nm excimer laser pulses. The dependence of neutral products yield on the pulse energy is indicated by the linear fits in this and subsequent log-log plots. . . . .	108
5.6	Protonated anthracene photodissociation with $\lambda = 248$ nm excimer laser pulses. .	109
5.7	Protonated pyrene photodissociation with $\lambda = 193$ nm excimer laser pulses. .	110
5.8	Estimates of dissociation energy for protonated anthracene by multiphoton nanosecond laser excitation. . . . .	111
6.1	A mass spectrum of the two-nozzle source of protonated anthracene–water clusters. . . . .	118
6.2	The benzene–water ( $\text{C}_6\text{H}_6 \cdot \text{H}_2\text{O}$ ) dimer geometry. . . . .	119
6.3	Protonated anthracene–water ( $1\text{--C}_{14}\text{H}_{11}^+ \cdot \text{H}_2\text{O}$ ) cluster geometry. . . . .	120

6.4	Protonated anthracene–water ( $C_{14}H_{11}^+ \cdot H_2O$ ) cluster photodissociation spectrum. Top: The recorded spectrum and exponential+Lorentzian fit. Bottom: Data with the exponential rise to short wavelengths removed. . . . .	122
6.5	The expected protonated anthracene–water cluster photodissociation spectrum from comparisons with PAH and $PAH^+$ clusters. . . . .	125
A.1	Calculated benzene $C_6H_6$ IR vibrational spectrum. . . . .	169
A.2	Calculated protonated benzene $C_6H_7^+$ IR vibrational spectrum. . . . .	169
A.3	Calculated naphthalene $C_{10}H_8$ IR vibrational spectrum. . . . .	170
A.4	Calculated protonated naphthalene 1– $C_{10}H_9^+$ IR vibrational spectrum. . . .	170
A.5	Calculated protonated naphthalene 2– $C_{10}H_9^+$ IR vibrational spectrum. . . .	171
A.6	Calculated anthracene $C_{14}H_{10}$ IR vibrational spectrum. . . . .	172
A.7	Calculated protonated anthracene 1– $C_{14}H_{11}^+$ IR vibrational spectrum. . . .	172
A.8	Calculated protonated anthracene 2– $C_{14}H_{11}^+$ IR vibrational spectrum. . . .	173
A.9	Calculated protonated anthracene 9– $C_{14}H_{11}^+$ IR vibrational spectrum. . . .	173
A.10	Calculated phenanthrene $C_{14}H_{10}$ IR vibrational spectrum. . . . .	174
A.11	Calculated protonated phenanthrene 1– $C_{14}H_{11}^+$ IR vibrational spectrum. . . .	174
A.12	Calculated protonated phenanthrene 2– $C_{14}H_{11}^+$ IR vibrational spectrum. . . .	175
A.13	Calculated protonated phenanthrene 3– $C_{14}H_{11}^+$ IR vibrational spectrum. . . .	175
A.14	Calculated protonated phenanthrene 4– $C_{14}H_{11}^+$ IR vibrational spectrum. . . .	176
A.15	Calculated protonated phenanthrene 9– $C_{14}H_{11}^+$ IR vibrational spectrum. . . .	176
A.16	Calculated pyrene $C_{16}H_{10}$ IR vibrational spectrum. . . . .	177
A.17	Calculated protonated pyrene 1– $C_{16}H_{11}^+$ IR vibrational spectrum. . . . .	177
A.18	Calculated protonated pyrene 2– $C_{16}H_{11}^+$ IR vibrational spectrum. . . . .	178
A.19	Calculated protonated pyrene 4– $C_{16}H_{11}^+$ IR vibrational spectrum. . . . .	178

B.1	Pulsed discharge source. . . . .	191
B.2	Ground (outside) pulsed discharge electrode. . . . .	192
B.3	High voltage (inside) pulsed discharge electrode. . . . .	193
B.4	Teflon insulating spacer between discharge electrodes. . . . .	194
B.5	PEEK insulating spacer between inside electrode and pulsed valve. . . . .	195
B.6	Electrode inserts for screw insulation. . . . .	196
B.7	Screw washer for insulation form outside electrode. . . . .	197
B.8	Pulsed discharge cluster source with two pulsed valves. . . . .	198
B.9	Ground (outside) discharge electrode for cluster production. . . . .	199
B.10	Non-discharge pulsed valve faceplate flange for cluster production. . . . .	200
B.11	TTL pulse width selector circuit, triggered by a TTL pulse rising front. . . .	201
B.12	Pulsed valve driver circuit. . . . .	203
B.13	One channel of the TOF MS high voltage pulser. . . . .	204
B.14	TOF MS pulser high voltage pulse profile (full). . . . .	205
B.15	TOF MS pulser high voltage pulse profile (front). . . . .	205
B.16	TTL triggering frequency divider. . . . .	207

## List of Tables

A.5	Protonated naphthalene (1-C <sub>10</sub> H <sub>9</sub> <sup>+</sup> ) Z-Matrix. . . . .	140
A.6	Protonated naphthalene (2-C <sub>10</sub> H <sub>9</sub> <sup>+</sup> ) Z-Matrix. . . . .	141
A.7	Anthracene (C <sub>14</sub> H <sub>10</sub> ) Z-Matrix. . . . .	142
A.8	Protonated anthracene (1-C <sub>14</sub> H <sub>11</sub> <sup>+</sup> ) Z-Matrix. . . . .	143
A.9	Protonated anthracene (2-C <sub>14</sub> H <sub>11</sub> <sup>+</sup> ) Z-Matrix. . . . .	144
A.10	Protonated anthracene (9-C <sub>14</sub> H <sub>11</sub> <sup>+</sup> ) Z-Matrix. . . . .	145
A.11	Phenanthrene (C <sub>14</sub> H <sub>10</sub> ) Z-Matrix. . . . .	146
A.12	Protonated phenanthrene (1-C <sub>14</sub> H <sub>11</sub> <sup>+</sup> ) Z-Matrix. . . . .	147
A.13	Protonated phenanthrene (2-C <sub>14</sub> H <sub>11</sub> <sup>+</sup> ) Z-Matrix. . . . .	148
A.14	Protonated phenanthrene (3-C <sub>14</sub> H <sub>11</sub> <sup>+</sup> ) Z-Matrix. . . . .	149
A.15	Protonated phenanthrene (4-C <sub>14</sub> H <sub>11</sub> <sup>+</sup> ) Z-Matrix. . . . .	150
A.16	Protonated phenanthrene (9-C <sub>14</sub> H <sub>11</sub> <sup>+</sup> ) Z-Matrix. . . . .	151
A.17	Pyrene (C <sub>16</sub> H <sub>10</sub> ) Z-Matrix. . . . .	152
A.18	Protonated pyrene (1-C <sub>16</sub> H <sub>11</sub> <sup>+</sup> ) Z-Matrix. . . . .	153
A.19	Protonated pyrene (2-C <sub>16</sub> H <sub>11</sub> <sup>+</sup> ) Z-Matrix. . . . .	154
A.20	Protonated pyrene (4-C <sub>16</sub> H <sub>11</sub> <sup>+</sup> ) Z-Matrix. . . . .	155
A.21	Scaling of the benzene molecule vibrational frequencies. . . . .	156
A.22	Scaling of the anthracene molecule vibrational frequencies. . . . .	157
A.23	Benzene and protonated benzene: scaled vibrational frequencies and IR intensities. . . . .	158
A.24	Naphthalene and protonated naphthalene: scaled vibrational frequencies and IR intensities. . . . .	159
A.25	Anthracene and protonated anthracene: scaled vibrational frequencies and IR intensities. . . . .	161

A.26	Phenanthrene and protonated phenanthrene: scaled vibrational frequencies and IR intensities. . . . .	163
A.27	Pyrene and protonated pyrene: scaled vibrational frequencies and IR intensities. . . . .	167
A.28	Protonated benzene energy landscape. . . . .	179
A.29	Protonated naphthalene energy landscape. . . . .	179
A.30	Protonated anthracene energy landscape. . . . .	180
A.31	Protonated phenanthrene energy landscape. . . . .	180
A.32	Protonated pyrene energy landscape. . . . .	180
A.33	Hydrogenated benzene energy landscape. . . . .	181
A.34	Hydrogenated naphthalene energy landscape. . . . .	181
A.35	Hydrogenated anthracene energy landscape. . . . .	182
A.36	Ionization energies for PAHs, hydrogenated and dehydrogenated PAHs. . . . .	183
A.37	Calculated first singlet excited states of neutral and protonated PAHs. $S_1$ state energies, $S_1 \leftarrow S_0$ wavelengths, red shifts, oscillator strengths. . . . .	184
A.38	Symmetry and $S_0$ , $S_1$ electronic states assignment for neutral and protonated PAHs. . . . .	185
A.39	Highest occupied (HOMO) and lowest unoccupied (LUMO) molecular orbitals of neutral and protonated PAHs. . . . .	186